Behavior of Tunnels against the Reverse Faulting Deformations Using Centrifuge Test and Numerical Modelling

Hamid Tohidifar[1], Mojtaba Moosavi[2], and Mohammad Kazem Jafari[3]*

1. Ph.D. Student, International Institute of Earthquake Engineering and Seismology (IIEES), Tehran, Iran
2. Assistant Professor, Geotechnical Engineering Research Center, International Institute of Earthquake Engineering and Seismology (IIEES), Tehran, Iran,
* Corresponding Author; email: moosavi@iiees.ac.ir
3. Professor and President, Geotechnical Engineering Research Center, International Institute of Earthquake Engineering and Seismology (IIEES), Tehran, Iran

Received: 28/12/2019
Accepted: 09/02/2020

ABSTRACT

The permanent ground deformation during the earthquake faulting induces moderate to severe damages to the underground tunnels. The majority of the investigations on the behavior of the tunnels against fault offset were in the rock medium. There is very little available in the literature about the fault-tunnel interaction in alluvial soil. This paper has studied the interaction between a continuous tunnel and reverse faulting within a dense sandy alluvial deposit. An experimental centrifuge test, alongside the numerical modelling, has been utilized for this purpose. It has been shown that the longitudinal strains of an infinite tunnel were much higher than that of a finite length tunnel. The results have also displayed that there are critical cross-sections along the tunnel's length that maximum curvatures, moments, shears, and axial forces occur in them. The numerical parametric study on the variation of the Fault Zone Width (FZW) and reinforcement content (ρ_s) have shown that higher ρ_s values would be more useful in tunnel resistance against faulting. Besides, smaller FZW will make higher deformations, moments, and forces in the concrete lining. The optimum ρ_s value has been obtained as 4%.

Keywords:
Tunnel; Alluvium;
Reverse fault rupture;
Centrifuge modelling;
Numerical modelling

1. Introduction

The rapid development of modern cities is dependent on substructures, which indeed play a pivotal role in supporting the fundamental needs of the communities. One of these vital substructures which used in the transportation of people or conveying water, wastewater, and energy over long distances is the underground tunnel. Extreme ground events such as the earthquake shaking or the earthquake faulting may affect the tunnels constructed in the seismically active regions. Tunnels in these regions should not only design for normal operating conditions but also should consider the extra loads and displacements in earthquake events.

The Permanent Ground Deformations (PGD) due to the earthquake faulting is one of the main events that affect the performance of embedded tunnels. PGD induces moderate to severe damages to the tunnels lining. The relocation of the underlying bedrock fault is the source of the extra forces imposed on the lining. To date, the greater part of the literature on the tunnel-earthquake interaction was on the effects of the seismic waves on the tunnels [1-8]. Past well-known earthquakes such as

the San Francisco [9], Idu Peninsula [10], Fukui [11], Kern County [12], Niigata [11], Off-Izu Oshima [13], Mid-north Iwate [14], and Duzce [15] have shown that PGD due to earthquake faulting could also severely damage the underground tunnels. Unfortunately, there is very little available about surface fault rupture influences on the tunnels [16-20]. Besides, amongst these little studies, even much less technical data could be found about the tunnels in alluvial deposits under dip-slip faulting. The existing data have concentrated mainly on tunnels surrounded within the rock media influenced by the strike-slip fault dislocations [11, 21-28]. Such studies, therefore, have failed to address the alluvial tunnels intersected by normal or reverse fault rupture planes (e.g. urban metro or motorway tunnels constructed in sandy deposits).

Brown et al. [29] provided a useful review of the behavior of different tunnels during the fault dislocations. The majority of the tunnels they have considered were constructed in rock materials bisected due to the movements of the strike-slip faults. The primary purpose of the Brown et al. [29] report was to study the behavior of Berkeley-Hill Bart tunnels through the Hayward fault. There is an elementary axisymmetric elastic finite element analysis in their report that by somehow reproduced the deformed shape of the Bart tunnel (Figure 1a). It was the first application of the numerical method in the fault-tunnel interaction problem.

Burridge et al. [16] have studied the behavior of the Los Angeles Metro Tunnel during the displacement of a 45° reverse fault that crossed the tunnel with right-angles. They have utilized the geotechnical centrifuge and one-dimensional Finite Element Method (FEM) for this investigation (Figure 1b and 1c). The purpose of employing numerical modelling in their work was to model an infinite tunnel in the soil (Figure 1c). This is because of the limited dimensions of their centrifuge container that prevented the modelling of a sufficiently long tunnel (Figure 1b). An elastic beam on simple elastoplastic springs has been used in their numerical modelling (Figure 1c). In centrifuge tests, an Aluminum tube has been used as the small-scale model of a prototype concrete tunnel. This model tube has simulated a tunnel with 5.34 m inside diameter and 0.2 m wall thickness. Due to the

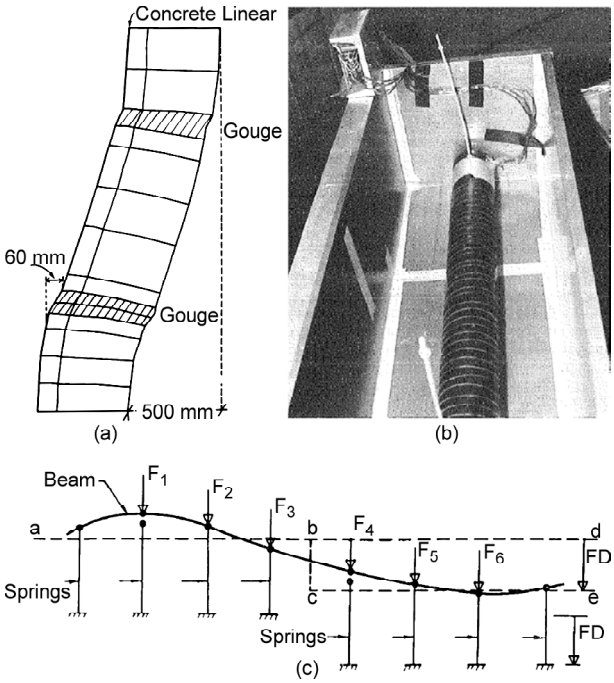

Figure 1. (a) Deformed mesh of the finite element model of Bart tunnel under strike-slip creep of Hayward fault, California; (b) model tunnel placed at right angles to fault in a split fault rupture centrifuge box [16]; (c) elastic beam on elastoplastic discrete spring foundation used in modeling Los Angeles Metro tunnel [16].

difficulties in the manufacturing of the model tunnel and its financial costs, the behavior of the Aluminum tunnel has been kept in the linear-elastic region. Furthermore, due to the different mechanical behavior of the Aluminum and concrete, the obtained results by Burridge et al. [16] did not demonstrate the real behavior of the concrete tunnel. Therefore, their results should be interpreted with caution.

In 1999, the uncompleted Bolu tunnel in Turkey damaged heavily due to ground shaking of the Duzce Earthquake [14-15]. Later investigations have revealed that the Bakacak fault would impose a distributed displacement up to 50 cm to this tunnel. Therefore, it was necessary to design the Bolu tunnel for this prospective fault-rupture. The response of the Bolu tunnel to the Bakacak fault displacement could be obtained through modelling the tunnel as a beam that its boundaries placed under the movements of the Bakacak fault [15]. A series of simplified elastoplastic springs might simulate the mechanical behavior of the surrounding soil. Although the beam-spring model has been suggested in Russo et al. [15], they have not provided any result of their numerical analyses.

The concept of the beam surrounded by elastoplastic springs has been first introduced by ASCE [30] and later by ALA [31] Guidelines. Both Guidelines were prepared for the analysis of the buried pipelines under the fault displacements. For tunnels in fault zones, FHWA-NHI-10-034 [32] and MCEER-06-SP11 [33] have suggested employing the same beam-spring model as proposed by ASCE [30] Guideline.

Lin et al. [20], Baziar et al. [34], and Mamaghanian et al. [35] have investigated the deformation of both tunnel and surrounding soil in the two-dimensional plane-strain condition (Figure 2a). These studies have revealed that the presence of a rigid or flexible tunnel within the alluvium could bifurcate the shear zone band emanated from the bedrock fault. Hence, the deformational pattern of the ground surface would alter due to the presence of the tunnel.

To investigate the role of tunnel boundary conditions, tunnel length, and tunnel depth on the stress-strain behavior of the lining, Cai et al. [18] conducted centrifuge tests and numerical analyses under the condition of normal faulting (Figure 2b). The relative orientation between the tunnel and the fault trace was 90°. The influence of boundary conditions on tunnel response was insignificant for a length longer than a specific value (700 m in their study). The results also showed that increasing the depth of the tunnel will increase the tunnel's longitudinal strains during the normal faulting. It should be noted that in Cai et al. [18], the tunnel behavior in both centrifuge models and numerical analyses were considered to be linear elastic.

It has been noted before that there is very little available in the literature regarding the tunnels constructed in the soil and subjected to the active fault displacements. In all the studies reviewed here about the effects of faults on the alluvial tunnels, however, what is not yet clear is the effect of the Fault Zone Width (FZW) on the concrete lining behavior. Besides, there are no previous reports in the literature on the influence of the rebar content on the response of the tunnels to the fault rupture. Thus, the objective of the present investigation is to find the effects of the FZW and rebar percentage on the maximum bending moments, forces, and strains in the lining of a typical tunnel. It is assumed that this tunnel has been constructed in sandy soil and subjected to a 60° reverse faulting. To this end, a numerical program, which developed by authors at IIEES, has been employed. This program validated and verified by the results of the centrifuge tests performed at IIEES by the authors and by Cai et al. [18].

2. A Numerical Method for Analyzing of Alluvial Tunnels Against Reverse Fault Displacements

Since 1980, different numerical methods have been employed to analyze the tunnel and fault rupture interaction [16, 18, 20, 29, 34, 36-38]. Finite element, finite difference, and discrete element methods have been used for this purpose. Moreover, it should be noted that the analytical methods developed for the buried pipelines could also be used in evaluating fault-tunnel interaction [39-41]. However, according to MCEER-06-SP11 [33], one should consider the overestimations that these analytical methods will impose on the results of the

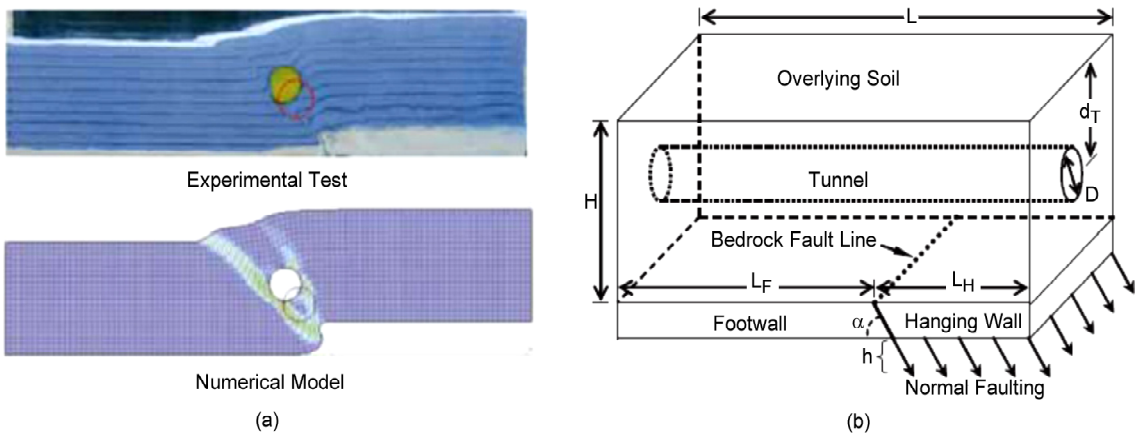

Figure 2. (a) The development of the fault zone in a two-dimensional plane strain problem [20] and, (b) The geometrical properties of a centrifuge test on a model aluminum continuous tunnel [18].

concrete tunnels.

The interaction between a tunnel and the surrounding soil could be modeled using either methods: beam-spring or three-dimensional continuum approach. Due to some problems such as the modeling complexities, convergence problems, severe increasing of the degrees of freedom, problems in introducing the contact elements between tunnel and the soil, difficulties in fault rupture modeling, and many computational efforts required in continuum approach, FHWA-NHI-10-034 [32] and MCEER-06-SP11 [33] have recommended to use the beam-spring method for the analyzing of the fault-tunnel interaction (Figure 3a and 3b). In this method, the tunnel is discretized into several beam-elements; each could take into account the axial, shear and bending deformations (Figure 3b). These elements can provide stresses and strains across the cross-sections along the tunnel axis. The material and geometrical nonlinearity could be incorporated into these elements. The surrounding soil, in this approach, is substituted by a series of soil-equivalent nonlinear springs (Winkler type), which are connected to each node of the modeled beam. Figure (3c) displays the mechanical behavior of these springs, which is elastic-perfectly-plastic. Furthermore, they are just working in compression mode and are tension-free springs.

In this paper, a series of studies on the behavior of the continuous tunnels with reinforced lining has been performed. The tunnels constructed in the soft ground (sandy soil) and subjected to the reverse fault movement (60° dip-angle). The beam-spring method has been utilized in this study. In addition, the finite-difference numerical approach has been used for the discretization of the beam elements in the tunnel. An in-house computer program has been developed in IIEES for the numerical studies of the tunnel-fault interaction. This program could consider both the material and geometrical nonlinearity. A detailed description of this program along with the beam-spring and the finite difference methods are available in Tohidifar et al. [42].

3. Verification of the Finite Difference Code with Normal Faulting Centrifuge Tests of Cai et al. [18]

In the Introduction section of this paper, it has been shown that Cai et al. [18] have performed two centrifuge tests to study the behavior of continuous tunnels subjected to normal faulting (Figure 2b). In order to verify the accuracy of the results of the above-mentioned finite difference code with a practical case, the beam-spring model of Cai et al. [18]'s experimental tests have been constructed in this paper. The tunnel dimensions and material properties for numerical analyses were adopted the same as the centrifuge tests (Table 1). The

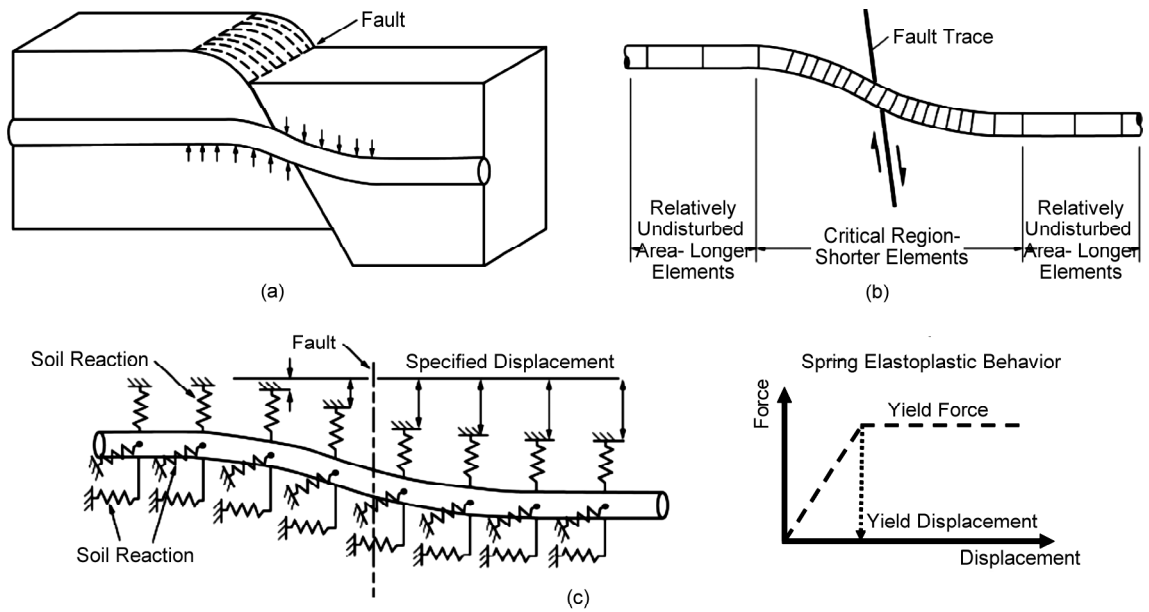

Figure 3. (a) the actual problem of the tunnel and a dip-slip fault intersection; (b) the simplification of the tunnel-fault problem for numerical modeling; (c) The soil-equivalent springs around the embedded beam and simplified mechanical behavior of springs. Tunnel substituted with a beam [30, 32].

Table 1. Dimensions and material properties necessary for the numerical analyses in the verification section (Data based on Cai et al. [18]).

Parameter	Numerical model	Prototype
Outer Diameter (m)	0.1	5
Tunnel Thickness (m)	0.003	0.36
Length (m)	1.15	57.5
Tunnel Elastic Modulus (GPa)	70	33
Bending Stiffness (kN.m^2)	75.3	4.71×10^8
Soil Friction Angle (Degrees)	31	31
Soil Unit Weight (kN.m^{-3})	15.33×50	15.33
Tunnel Embedment Depth (m)	0.15	7.5
	0.25	12.5
Fault Type	**Normal - 70°**	
Fault Vertical Displacement (cm)	1.6	80
L_H (m) - Figure 2b	0.382	19.1
L_F (m) - Figure 2b	0.788	39.4

Table 2. Spring properties necessary for the numerical analyses in the verification section based on the ASCE [30].

Spring Type	d_T = 7.5 m		d_T = 12.5 m	
	Yield Force (kN/m)	Yield Displacement (mm)	Yield Force (kN/m)	Yield Displacement (mm)
Axial	10.67	2.4	17.8	2.4
Vertical Bearing	320	7.3	480	7.3
Vertical Upward	10.36	2.4	28.8	2.4

centrifugal acceleration was 50 g. Therefore, the soil unit-weight has been multiplied by a 50 factor to similitude the real overburden pressure on the model tunnel (Table 1). The axial, Transverse-vertical-bearing and vertical-upward spring properties were derived according to the ASCE [30] Guideline. These elastic-perfectly-plastic springs were characterized by a yield displacement and a yield force. For two separate centrifuge tests with varying embedment depths, these spring properties have been obtained as Table (2).

Figure (4) shows the comparison between the longitudinal strains induced at the tunnel crown during the final displacement of the fault. It can be seen in this figure that there is a good agreement between the experimental and numerical results. Therefore, the developed finite difference code has predicted the centrifuge experimental data appropriately.

4. Centrifuge Test on a Tunnel under Reverse Faulting and verification of the numerical method

The behavior of tunnels, when subjected to the displacements of the reverse faulting, is completely different compared to the situation of the normal fault offsets. In general, there is limited information on the tunnel performance during the reverse faulting [16, 19, 20, 34]. Past experimental investigations just limited to the centrifuge tests of Burridge et al. [16], if tunnel-fault intersection angle is equal to 90 degrees. It has already been seen in the Introduction section that the scaled model tunnel of Burridge et al. [16] have been manufactured from Aluminum material. Because of the different stress-strain

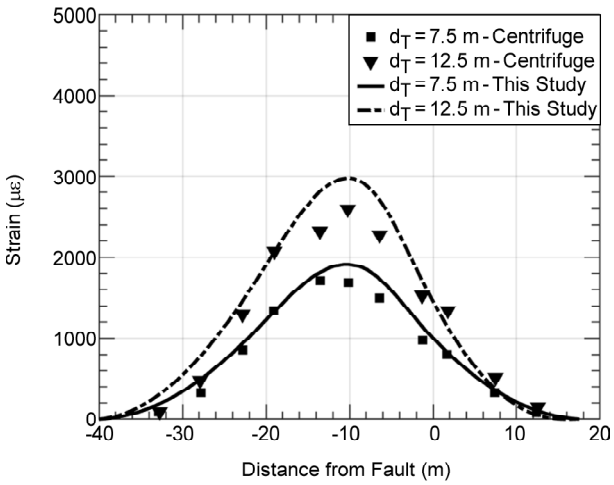

Figure 4. Comparison of the longitudinal strains at the crown of the tunnel for two embedment depths (d_T=7.5 & 12.5 m). Results are from the current study's numerical analyses and experimental measures by Cai et al. [18].

Table 3. Physical and mechanical characteristics of the Firoozkooh Sand No. 161.

USCS	Gs	F_c (%)	w_c (%)	D_{50} (mm)	e_{min}	e_{max}	D_r (%)	φ (°)	c (kPa)
SP	2.65	0	3	0.27	0.548	0.943	65	37	0

characteristics of Concrete and Aluminum, especially in the vicinity or after the concrete cracking, their results should be treated with care.

Moreover, the boundary conditions of the model tunnel in Burridge et al. [16] were such that they were neither free nor fix. In fact, the flexibility or rigidity of the boundary conditions was unknown. Due to these deficiencies, more investigations are necessary for this field.

In order to study the behavior of tunnels against reverse faulting more precisely, one centrifuge test has recently been performed by the authors at the advanced laboratory center of IIEES. The centrifuge gravitational acceleration, Ng, which defines the scaling factor of the linear dimensions of the model to prototype (1/N), was equal to 25 g. The soil was Firoozkooh Sand No. 161 with the physical and mechanical properties presented in Table (3). For modelling of a concrete tunnel with 2.8 m outer diameter and 12.5 cm lining thickness, an asbestos cement pipe with 11.2 cm outer diameter and 6.5 mm thickness has been adopted. The length of this pipe in the centrifuge test was 63 cm (15.75 m in prototype scale). The modulus of elasticity of the concrete has been assumed to be 25 GPa. The same modulus for the asbestos cement pipe was 20 GPa.

The fault rupture split box for the geotechnical centrifuge tests was designed and manufactured in IIEES by the authors, recently (Figure 5). This device could simulate the action of a reverse fault with a 60° dip-angle. The dimensions of the soil container part of the box are 80 cm long, 70 cm wide, and 58 cm deep. It consists of a stationary floor (foot-wall) and a moving portion (hanging-wall) (Figure 5). The movement of the hanging-wall side is provided by the ramming force of a hydraulic-jack just placed in the backside of the right end-wall. The maximum allowable vertical displacement of this hanging-wall is 5 cm. For checking the deformation of the soil during the fault rupture and for taking consecutive pictures for the subsequent images processing, a Plexiglas plate with 4 cm thickness has been placed in front side of the box's container.

For modelling the tunnel-fault interaction, the soil depth in the box was considered to be 28 cm. Under 25 g gravitational acceleration, this depth simulated a sand deposit with 7 m height in prototype scale. The sand has been poured and compacted in seven layers. The thickness of each compacted layer was 5 cm, except that the last upper layer which had 3 cm thickness.

The left boundary of the model tunnel was placed inside a steel sleeve which extended to the adjacent end-wall (Figure 6). The inside diameter of this sleeve was greater than the outer diameter of the asbestos tunnel. Therefore, a strip of very compressible polyethylene foam with annular shape

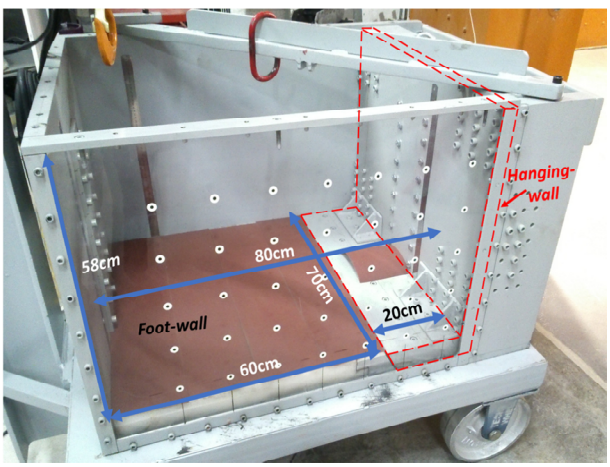

Figure 5. Fault-rupture split box, designed and manufactured for the advanced geotechnical laboratory of IIEES.

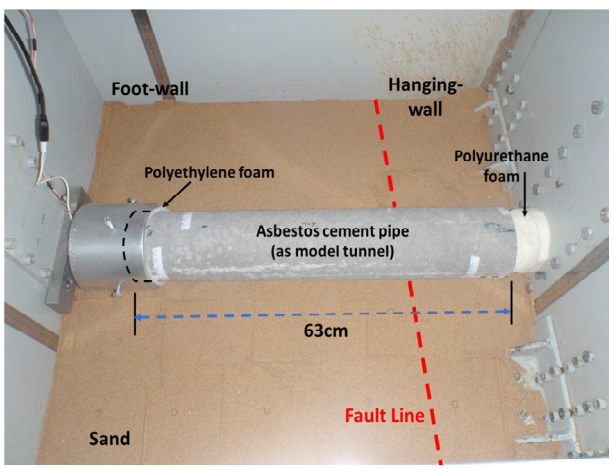

Figure 6. The model tunnel (asbestos cement pipe) placed inside the split-box.

was placed between sleeve and pipe. In this case, the model tunnel could rotate and displace without any resistance inside this boundary (free boundary). For the right boundary in the hanging-wall side, the model asbestos tube was placed over a solid cylindrical polyurethane foam. This flexible foam could glide smoothly inside the tunnel. As illustrated in Figure (6), the cylindrical foam was extended to the right end-wall. Therefore, during the fault movements, due to the flexibility and compressibility of this foam, the right boundary of the model tunnel simulated the free condition.

The model tunnel was placed at a depth of the 4.9 m (prototype scale) from the ground surface (central tunnel axis to the surface). The fault's vertical displacement was 4 cm in model scale and 1 m in real scale.

Figure (7a) shows the deformed shape of the model tunnel after the 4 cm vertical displacement of a reverse fault (model scale). A rigid body motion, including rigid displacement and rigid rotation, has been obtained for the model tunnel. Three factors were responsible for this rigid movement. These are (1) the finite length of the model tunnel, (2) the free boundary conditions at either side of the asbestos cement pipe, and (3) the higher stiffness of the pipe to the surrounding soil. Further inspections of the pipe after the test have revealed that there was no sign of any cracks or spalling in the model tunnel. Therefore, the model tunnel has worked in the linear-elastic range.

For better understanding the behavior of this tunnel, a numerical study has also been performed. The elastic modulus of the tunnel in numerical analysis was the same as the asbestos cement's one (i.e. 20 GPa). Besides, the lining material behavior was assumed to be elastic. Soil equivalent spring characteristics have obtained in Table (4). Figure (7b) presented the spectrum of the longitudinal strains along the tunnel. The maximum and minimum

Table 4. Spring properties for the numerical analysis of IIEES centrifuge test.

Spring Type	d_T = 4.9 m	
	Yield Force (kN/m)	Yield Displacement (mm)
Axial	9.2	1.6
Vertical Bearing	7.37×10^3	6.4
Vertical Upward	11.6	1.3

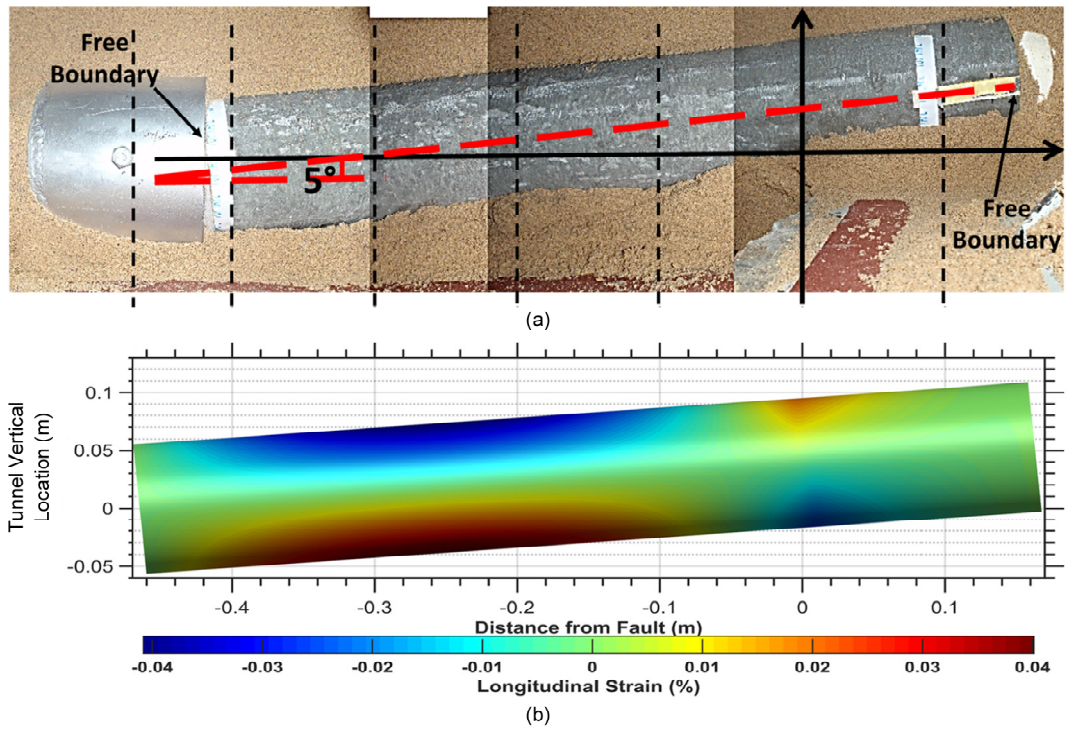

Figure 7. (a) Deformation of model tunnel after centrifuge test due to 4 cm vertical displacement of fault, and (b) the longitudinal strain spectrum of the tunnel obtained from numerical analysis.

longitudinal strains based on this figure was 0.04% and -0.04%, respectively. The onset of compressive yielding of the concrete based on fib [43] is -0.175%. This value is higher than the -0.04% developed in the tunnel lining. Therefore, the tunnel has not yielded or crushed in compression mode.

On the other hand, the tensile failure of a concrete with occurs at a strain equal to 0.014% [44]. This value is lower than the +0.04% created in the lining of the model tunnel. Therefore, tension cracks should be developed in the prototype concrete tunnel. Consequently, tunnel requires longitudinal reinforcements to bear this tension strain.

The rotation angle of the tunnel in Figure (7a) was 5°. The numerical analysis predicted this rotation as 4.8° through the entire length of the tunnel. Therefore, the rigid body motion of the model tunnel has also been shown in the numerical analysis.

The limited dimensions of the split box have precluded to model a prototype tunnel with essentially infinite length. The calibrated numerical model with above centrifuge test could be helpful in modelling of an infinite prototype tunnel. Therefore, a real tunnel with 2.8 m outer diameter, 12.5 cm lining thickness, and 900 m length was modelled in the same embedment depth as above. A 60° reverse fault with 1 m vertical displacement has been imposed on the tunnel. For the comparison with the results of the model tunnel in the centrifuge test, the yielding and failure of the lining material have been prevented. Therefore, linear elastic material was used again in this analysis.

Figure (8) demonstrated the longitudinal strains in the top and bottom fibers of the tunnels modelled numerically in this study (i.e. centrifuge test model and infinite tunnel). It is evident from this figure that the effect of the boundary conditions on the magnitude of the developed strains was significant. The maximum tensile and compressive strains in the top fiber of the infinite tunnel were 35 and 19.5 folds greater than the same strains of the centrifuge tunnel, respectively. These values for bottom fiber were 9.75 and 42.3. Moreover, the magnitude of the tensile and compressive strains in the infinite tunnel was such that the compression and tensile failure of the lining concrete would occur by 1 m displacement of the fault.

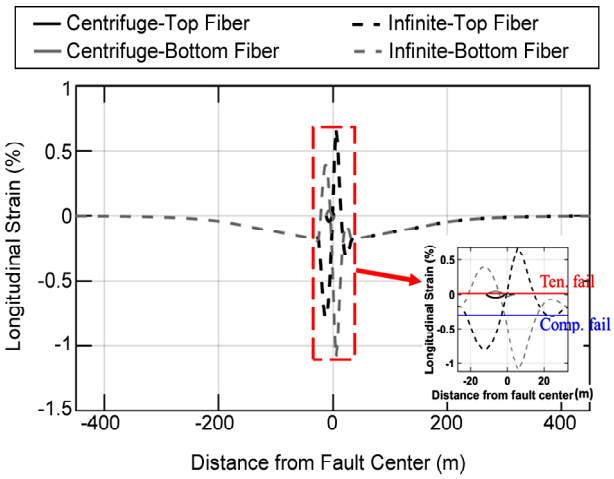

Figure 8. Development of the longitudinal strain in the top and bottom fiber of the prototype tunnels.

5. Numerical Analyses of Tunnel under Reverse Faulting (Parametric Study)

To address the behavior of cast-in-place reinforced concrete tunnels constructed in sandy deposits and subjected to the reverse faulting, a parametric study has been performed in this paper on the circular tunnels. It was assumed that the tunnel had a length equal to 300 m and was under a 60° reverse fault offset (Figure 9a). The Fault Zone Width (FZW) in the middle portion of the tunnel had a length equal to 5, 10, and 50 m (Figure 9a and 9b). A hyperbolic distribution for both vertical and horizontal PGD has been assumed (Figure 9b). If the maximum vertical PGD is considered to be equal to δ, then because of the 60° reverse fault displacement, the maximum horizontal PGD would be $cot\,\delta(60°)$.

The cross-section of the tunnel was a tube-liked reinforced concrete section that according to section A-A in Figure (9a) has been schematized in Figure (9c). The unconfined cylindrical compressive strength of the concrete at the age of 28 days has been considered to be $f_c' = 25\text{MPa}$. The longitudinal and shear reinforcements had a maximum yield strength equal to 420 MPa and an elastic Young's modulus equal to 200 GPa (US steel grade 60). The stress-strain curve of the concrete and the steel materials that have been used in this numerical analysis are presented in Figure (10). These simplified curves have been suggested by different Standards and Guidelines such as TEC [45], fib [43], Eurocode2 [46] and ITA [47].

The tunnel outer diameter has been assumed to

be 6 m (Figure 9c). This diameter corresponds to a single-track train or metro tunnel. Besides the concrete lining thickness has been considered to be equal to 30 cm, which satisfies the minimum thickness conditions of ITA [48] and O'Rourke [8]. The embedment depth of the tunnel has been supposed to be 10 m. This depth indicates that the type of examined tunnel was shallow.

The concrete cover for reinforcements at the outer and inner surfaces of the circular tunnels was 8 cm and 5 cm, respectively (Figure 9c) [48-49].

The ratio of the total cross-sectional area of the longitudinal reinforcements to the gross area of the concrete tunnel has been assumed to be ρ_s = 0.5, 1.5 and 4%. The total cross-sectional area of both longitudinal and shear reinforcements are also higher than the minimum values proposed by the International Tunneling Association [48] as demonstrated in Table (5).

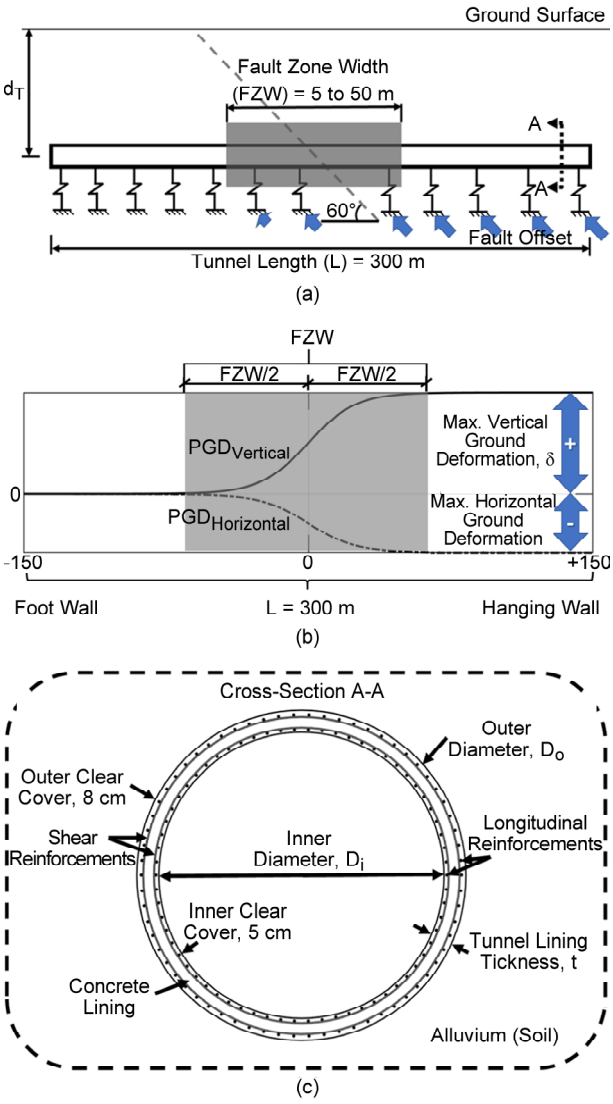

Figure 9. (a) Longitudinal view of the modeled tunnel in the soil. Springs are worked in axial, vertical downwards and upwards but for graphical reasons not shown here; (b) the distribution of the permanent ground deformation in the vertical and horizontal directions and the fault zone; (c) A-A cross-section of the modeled Tunnel.

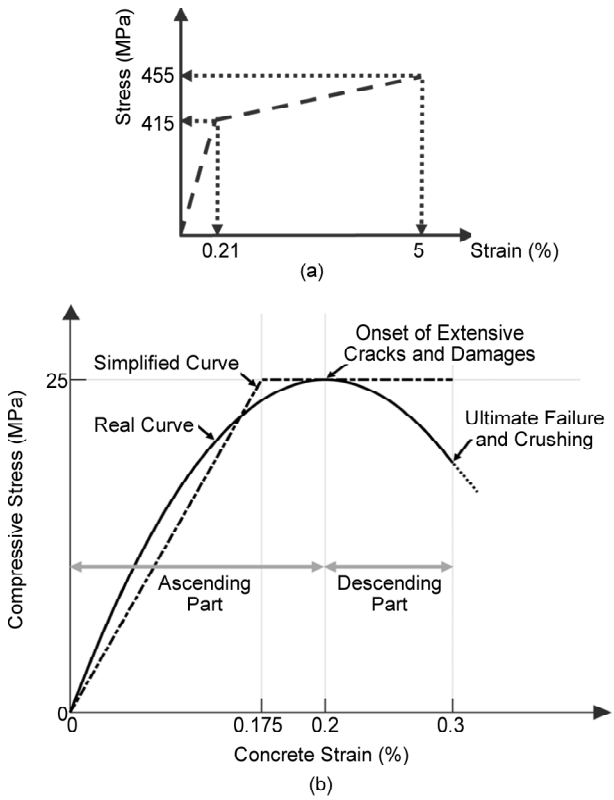

Figure 10. Simplified stress-strain curves for, (a) reinforcing steel, and (b) concrete. According to fib [43] and ITA [47].

Table 5. Amount of longitudinal and shear reinforcements for tunnels in the current study

t			30 cm		
Rein. Type			Longitudinal		Shear
Surface position			I (cm^2/m)	O (cm^2/m)	I & O (cm^2/m)
D_o (m)	6	ρ_s=0.5%	7.3	7.8	15.7
		ρ_s=1.5%	22.0	23.3	
		ρ_s=4.0%	58.6	62.2	

I: Inner surface; O: Outer Surface.
Minimum required reinforcements on the outer surface per International Tunneling Association [48]: 1.5 cm^2/m
Minimum required reinforcements on the inner surface per International Tunneling Association [48]: 3.0 cm^2/m

The analyzed tunnel has been assumed that bored in a soft ground medium. This soft ground was a dense sandy deposit with 40° friction angle and 17 kN/m3 unit weight density. It was also assumed that the ground is homogenous and isotropic. Therefore, a constant soil friction angle (i.e. 40°) has been used in the estimation of the capacity of the soil springs required in the beam-spring models. As already described, the definition of these equivalent nonlinear springs is leaned on the guidelines for the seismic design of oil and gas pipeline systems, ASCE [30].

The speed of execution is crucial in such numerical analyses. Therefore, a preliminary mesh length analysis has been accomplished to minimize computational costs. An optimum beam-element length equal to 2.5 m has been obtained, which for a 300 m long tunnel led to 121 equally spaced nodes along the modelled tunnel beam.

6. Fault Displacement Effects on the Bending Moment, Axial and Shear Forces

This section describes the nature of the development of the bending moments, axial and shear forces in a concrete tunnel induced by the permanent ground displacement. The profile of the vertical displace-ments of a tunnel with D_o = 6m, t = 0.3 m, dT = 10m, ρ_s = 1.5%, and FZW = 10 m is presented in Figure (11a). Four different levels of vertical fault offsets have been illustrated in this figure (i.e. δ = 3, 6, 9, and 12 cm). The pattern of these displacement curves is such that they are all showing an inflection point in the center of the fault region. The inflection point is a point that the curvature, κ, changes its sign from positive to negative or vice versa (Figure 12a). Based on the principles of structural analysis, the bending moment of a beam is dependent on its curvature magnitude (e.g. in elastic region $M = \kappa(EI)_t$). Therefore, the intersection of the bending moment curves with M = 0 line in Figure (11b), also show the point of inflection inside the fault zone.

The maximum magnitude of dM/dx occurs at the inflection point. Therefore, based on the principles of the mechanics of the materials [50], the maximum beam shear force should be placed at this point ($V = dM/dx$). Figure (11c) shows this matter clearly. Moreover, the shear forces were equal to zero when $V = dM/dx = 0$. The distribution of the axial forces along the tunnel has been demonstrated in Figure (11d). The maximum axial forces for

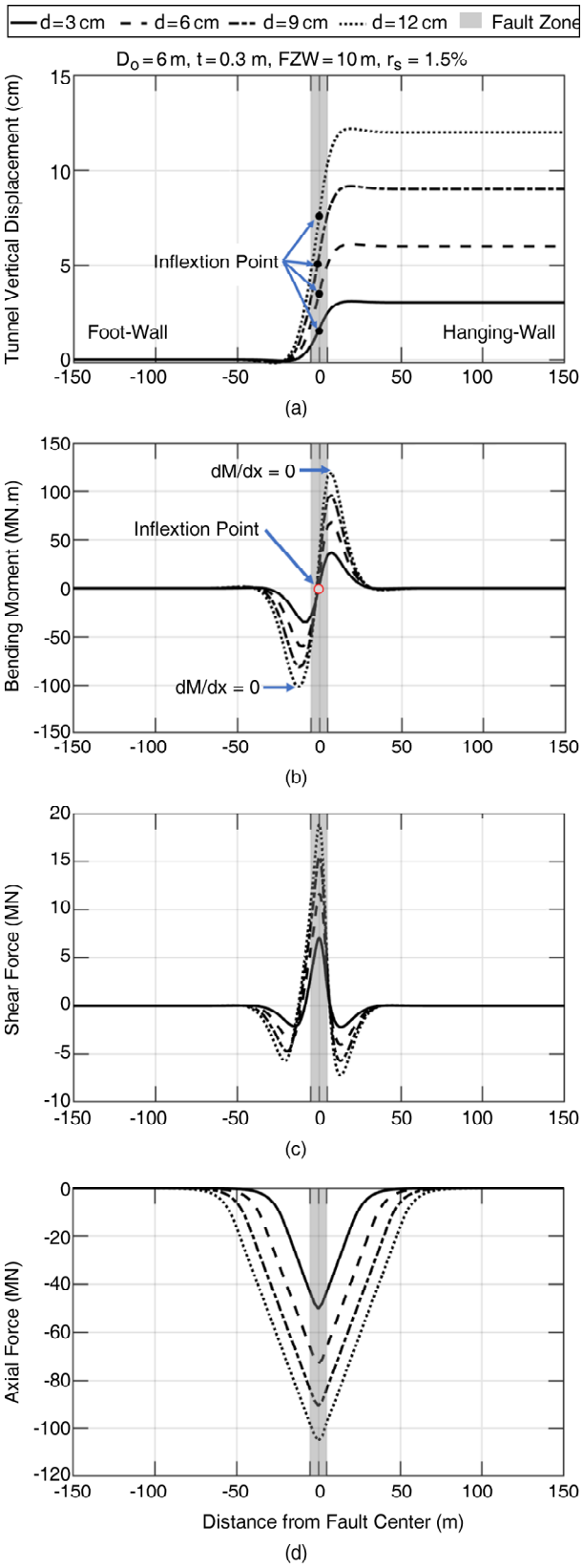

Figure 11. Variation of (a) vertical displacements; (b) bending moments; (c) shear forces; and (d) axial forces; for a tunnel with D_o = 6 m, t = 30 cm, ρ_s=1.5%, d_T=10 m, FZW=10 m.

different fault displacements occurred in the middle of the fault zone. The negative values of the axial forces show that the tunnel cross-sections were under compressive actions of the fault. This compression force is one of the main characteristics of reverse faults.

It is apparent from Figure (11b, 11c, and 11d) and Figure (12a) that bending moments, shear and axial forces, and curvatures were increasing functions of the fault displacement. It should be noted that the magnitudes of the bending moments, shear forces, and curvatures in the hanging wall side of the fault were higher than the footwall side. This finding will be explained in more details in the following paragraph.

Figure (12b) illustrated the general deflection curve of a tunnel against the reverse fault movement. If the inflection point of this tunnel is considered as a pivot that the sign of the curvature changes around it and exactly at this point $M = 0$ and $V = V_{max}$, then it could be assumed that there is an equivalent shear surface that passes by this point and divides the tunnel into two up-going and down-going sections. This figure shows that in the hanging-wall and foot-wall sides, the bearing and upward springs have been activated, respectively. Because the stiffness and the ultimate force of the bearing springs were higher than the upward ones, therefore, higher moments or shear forces have been created in the hanging wall in comparison to the footwall.

The location of the maximum moments, maximum shear, and maximum axial forces show that in designing process of the tunnels for fault crossing, there are critical sections that should be considered in the tunnel analysis. If no substantial ground movements imposed on the tunnel, then increasing the reinforcement ratio at these critical sections might be useful in diminishing the tunnel liner damages. This issue is discussed further in the next section.

7. Effects of Longitudinal Reinforcement Ratio ρ_s on Tunnel Response

In the previous section, the distribution of the bending moments, shear, and axial forces for a tunnel against fault displacements have been obtained for ρ_s = 1.5%. This section is concerned with the effects of the different ρ_s ratios (i.e. 0.5 and 4%) on the tunnel reactions against the surface fault rupture. The FZW in this section had a range from 5 to 50 m. The maximum fault displacement has been assumed to be $\delta = 15$ cm in the vertical direction. This displacement is equivalent to an earthquake with a moment magnitude, Mw, equal to 3.5 Richter [51].

As seen in Figure (13-a), the increasing of the reinforcement ratio caused a decrease in the maximum curvature values for FZW = 5 m. On the other hand, the maximum curvatures do not change substantially for FZW = 50 m. The graphs in Figure (13a) also show that by increasing the FZW, the magnitude of the maximum curvatures has been dropped drastically. These may be explained by two possible mechanisms: (1) the localization of ground displacements, and (2) the stiffness of the tunnel. The increase of the reinforcement ratio will cause increasing the tunnel stiffness. When the

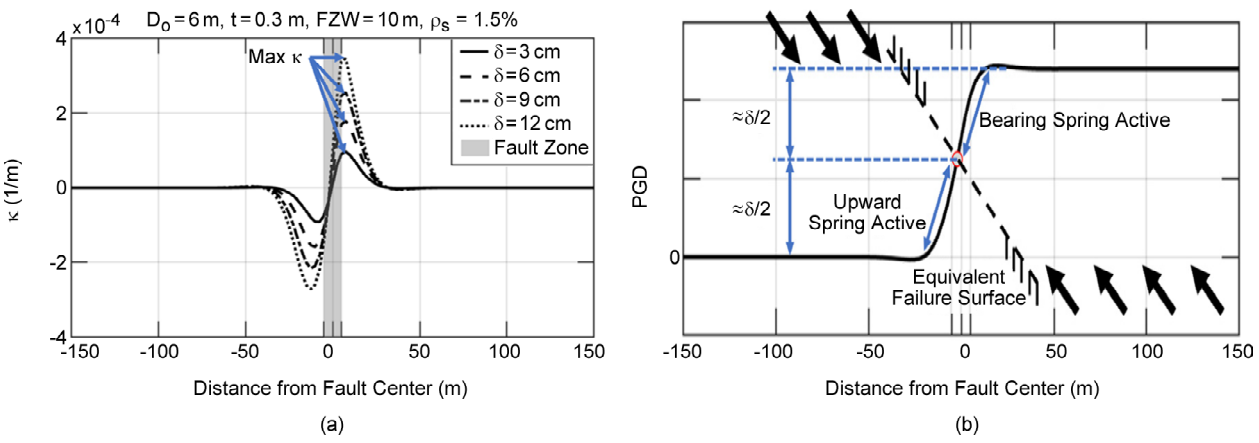

Figure 12. (a) Variation of curvature along the tunnel axis, and (b) the general concept of the tunnel deformation, equivalent failure surface, and the nature of the activation of the vertical springs.

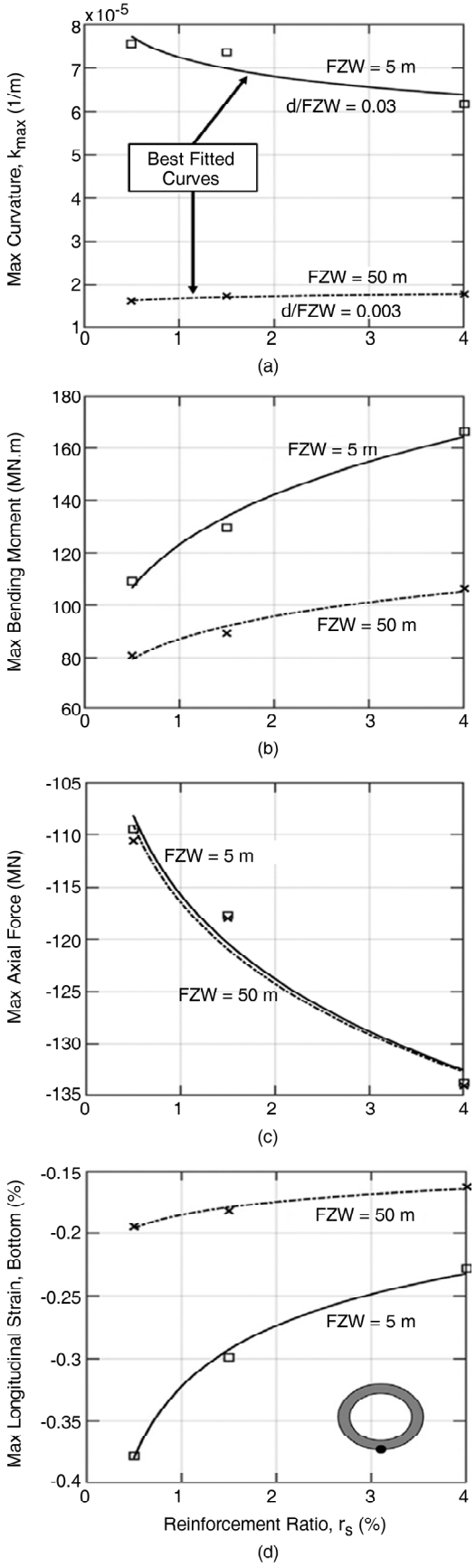

Figure 13. Variation of different tunnel parameters versus longitudinal reinforcement ratio ρ_s, (a) maximum tunnel curvature; (b) maximum bending moments; (c) maximum axial force; and (d) maximum longitudinal strain on the lower edge of tunnel's invert. (D_o = 6 m, t = 30 cm, d_T = 10 m, and FZW = 5 & 50 m)

localization of the ground movements is high, i.e. lower FZW or higher δ/FZW, the tunnels with lower stiffness will deform more conveniently. Therefore, more curvature along the tunnel axis will take place.

On the other hand, for the higher FZW, the width of the region of the ground displacements is such that for a constant vertical fault displacement, δ, the δ/FZW ratio is tenfold lower. Therefore, the same δ has been distributed in the broader zone. This lower angular ground deformation caused to the smaller tunnel curvatures.

The maximum bending moment diagrams for ρ_s = 0.5, 1.5, and 4% ratios and FZW = 5 and 50 m are presented in Figure (13b). The general trend of both FZW = 5 and 50 m curves is ascending. There is a specific ρ_s value after which the bending moment magnitudes will not change significantly. It was expected that for FZW = 5 m, the moments would be higher than FZW = 50 m. Referring to the preceding paragraph, the lower tunnel curvatures in FZW = 50 m have resulted in lesser magnitudes of the maximum moments. The higher ρ_s values cause to higher tunnel rigidity. Therefore, higher bending moments have been developed for more rigid tunnels

For the maximum axial force in the tunnels (Figure 13c), which occur within the middle section of the fault zone width (Figure 11d), there was no difference between the FZW = 5 and 10 m. The negative sign of these forces proves that the tunnels were under compression due to the reverse faulting. The trend of both curves was increasing by increasing of ρ_s in the compressive part of the chart. Also, similar to the maximum bending diagrams in Figure (13b), it seems that there is an asymptote in N_{max} = -135 MN that makes an upper-bound for the proposed curves. No significant changes in maximum axial forces will be happened by increasing ρ_s values higher than 4%.

The maximum longitudinal strain (bending+axial strains) in the lower edge of the tunnel's invert are presented in Figure (13d). In this study, this lower edge strains have been more critical than the upper edge of the tunnel's crown. Apparently, lower compressive strains have been induced in FZW = 50 m. As already explained, the lower δ/FZW ratio for FZW=50 m have indicated lower induced

deformations into the tunnel. Therefore, lower maximum curvatures, bending moments, and longitudinal strains have been obtained in this case. Conversely, the localization of the ground displacement in FZW = 5 m was higher. Hence, the developed strains were greater. The general trend of the maximum strain curves was decreasing by increasing of the ρ_s. However, the rate of this reduction was higher for the FZW = 5 m. This figure shows explicitly that the increase of the longitudinal reinforcement ratio would be quite useful in decreasing the strains and therefore the damages imposed to the tunnel lining. This effect is slighter for the wider fault zones (FZW = 50 m in this study). For FZW = 5 m, the difference in maximum com-pressive strain for ρ_s = 0.5% and ρ_s = 4% was 65%. It means that by δ = 15 cm, in a tunnel with D_o = 6 m, t = 30 cm, and d_T = 10 m, the induced strains with ρ_s = 4% were 65% lower than ρ_s = 0.5%. This diminution was 30% for ρ_s = 1.5% and ρ_s = 4%. In addition, there is an optimum ρ_s value after that the amount of the strain decreasing would not be sensitive to ρ_s. It is suggested equal to 4% in this study.

8. Conclusion

This study has identified the effects of the ground deformations due to the reverse faulting on the response of the continuous concrete tunnels. A computer program, which has been developed based on the finite difference method, has been employed for analyzing of the fault and tunnel interaction. This computer program was verified and validated through two experimental centrifuge tests performed at the IIEES' advanced laboratory center by the authors, and the tests carried out by Cai et al. [18]. The results of the IIEES centrifuge test and the subsequent numerical models have shown that the length of the tunnel has a significant and direct effect on the amount of the developed strains in the lining.

A numerical parametric study has also been performed in this paper. It was assumed that the examined tunnels have been bored in sandy deposits with cast-in-place reinforced concrete lining. The assumed tunnels had D_o = 6 m, t = 30 cm, d_T = 10 m, and ρ_s = 0.5, 1.5, and 4%. The Fault Zone Width (FZW) was assumed to be 5, 10, and 50 m. The results of the analyses have shown that the greater the ground displacements, the greater the bending moments, axial and shear forces, and curvatures. There was an inflection point in the tunnel deflection curves that in there the bending moments were zero and the shear forces were maximum.

The FZW had a significant influence on the maximum curvatures, bending moments, and longitudinal strains. The smaller the FZW, the more ground displacement localized. Therefore, more strains, moments, and curvatures have been obtained. Using a constant vertical ground displacement, δ, the δ/FZW ratio was lower for higher FZW. Therefore, relatively smaller angular deformations imposed on the tunnel liner. It shows that for wider FZWs, the maximum curvatures and moments were smaller.

The increase of the longitudinal reinforcement ratio, ρ_s, have made the tunnel stiffer and stronger. Due to stiffness increment, the maximum bending moments have been increased, while maximum longitudinal strains have been decreased. It shows that higher ρ_s magnitudes will be useful in decreasing the lining strains and therefore in mitigation of tunnel damages. It should be noted that there is a limit value for ρ_s (=4%) after which the increasing of ρ_s would not alter the strains, axial forces, curvatures, and bending moments, significantly. Consequently, ρ_s = 4% was an optimum value for the tunnels studied in this paper. Besides, for higher FZW (=50 m in this study), the variation of ρ_s did not make sharp differences in reduction of longitudinal strains or curvatures. Therefore, it is recommended to consider the δ, FZW, and ρ_s factors together in the estimation of the behavior of the continuous tunnels against the surface faulting action.

Acknowledgement

The financial support of the International Institute of Earthquake Engineering and Seismology (IIEES) under project number 6137 is gratefully acknowledged. In addition, authors would like to thank Mr. Kamran Shirazian for his assistance in carrying out the centrifuge test.

References

1. Hashash, Y.M., Hook, J.J., Schmidt, B., John, I.,

Yao, C. (2001) Seismic design and analysis of underground structures. *Tunnelling and Underground Space Technology*, **16**, 247-293.

2. Hashash, Y.M., Park, D., John, I., and Yao, C. (2005) Ovaling deformations of circular tunnels under seismic loading, an update on seismic design and analysis of underground structures. *Tunnelling and Underground Space Technology*, **20**, 435-441.

3. Anastasopoulos, I., Gerolymos, N., Drosos, V., Kourkoulis, R., Georgarakos, T., and Gazetas, G. (2007) Nonlinear response of deep immersed tunnel to strong seismic shaking. *Journal of Geotechnical and Geoenvironmental Engineering*, **133**, 1067-1090.

4. Anastasopoulos, I. Gerolymos, N. Drosos, V. Georgarakos, T. Kourkoulis, R., and Gazetas, G. (2008) Behaviour of deep immersed tunnel under combined normal fault rupture deformation and subsequent seismic shaking. *Bulletin of Earthquake Engineering*, **6**, 213-239.

5. St John,C. and Zahrah, T. (1987) Aseismic design of underground structures. *Tunnelling and Underground Space Technology*, **2**, 165-197.

6. Owen, G.N. and Scholl, R.E. (1981) Earthquake engineering of large underground structures. *Federal Highway Administration and National Science Foundation*.

7. Wang, J. (1993) Seismic design of tunnels: a state-of-the-art approach, monograph, monograph 7. Parsons, Brinckerhoff, Quade and Douglas Inc, New York.

8. O'Rourke, T.D. (1984) G*uidelines for Tunnel lining Design*. Technical Committee on Tunnel Lining Design of the Underground Research Council of the ASCE Technical Council on Research, p82.

9. Lawson, A.C. (1908) *The California Earthquake of April 18, 1906*. Report of the State Earthquake Investigation Commission, Carnegie Institution of Washington.

10. Takahasi, R. (1931) Results of the precise levellings excuted in the tanna railway tunnel and the movement along the Slicken-side that appeared in the tunnel. *Earthquake Research Institute Bulletin*, **9**, 435-453.

11. Dowding, C.H. and Rozen, A. (1978) Damage to rock tunnels from earthquake shaking. *ASCE J. Geotech. Eng. Div.*, **104**, 175-191.

12. Kupfer, D.H., Muessig, S., Smith, G., White, and Arvin-Tehachapi, G.N. (1955) Earthquake damage along the Southern Pacific railroad near bealville, California. *California Div., Mines Bull.*, **171**, 67-74.

13. Tsuneishi, Y., Ito, T., and Kano,K.-I. (1978) Surface faulting associated with the 1978 Izu-Oshima-kinkai earthquake. *Bulletin of Earthquake Research Engineering*, **53**, 649-674.

14. Konagai, K., Kunimatsu, S., Ueta, K., Uehan, F., Onizuka, N., Kiku, H., Suzuki, T., Nakase, H., Nozu, A., Matsushima, Johansson, T.J., Chen, C.-H., Lee, W.F., and Mei, T. (2006) K*ey Points for Rational Design for Civil-Infrastructures Near Seismic Faults Reflecting Soil-Structure Interaction Features*. Technical Committee for Fault-Related Geotechnical Issues about Civil-infrastructures, Japan Geotechnical Society (JGS).

15. Russo, M., Germani, G., and Amberg, W. (2002) Design and construction of large tunnel through active faults: a recent application. *Proceedings International Conference of Tunneling and Underground Space Use*, Istanbul.

16. Burridge, P.B., Scott, R.F., and Hall, J.F. (1989) Centrifuge study of faulting effects on tunnel. *Journal of Geotechnical Engineering*, **115**, 949-967.

17. Kiani, M., Akhlaghi, T., and Ghalandarzadeh, A. (2016) Experimental modeling of segmental shallow tunnels in alluvial affected by normal faults. *Tunnelling and Underground Space Technology*, **51**, 108-119.

18. Cai, Q., Peng, J., Ng, C.W., Shi, J., and Chen, X. (2019) Centrifuge and numerical modelling of tunnel intersected by normal fault rupture in sand. *Computers and Geotechnics*, **111**, 137-146.

19. Baziar, M.H., Nabizadeh, A., Lee, C.J.,

and Hung,W.Y. (2014) Centrifuge modeling of interaction between reverse faulting and tunnel. *Soil Dynamics and Earthquake Engineering*, **65**, 151-164.

20. Lin, M.-L., Chung,C.-F., Jeng,F.-S., and Yao,T.-C. (2007) The deformation of overburden soil induced by thrust faulting and its impact on underground tunnels. *Engineering Geology*, **92**, 110-132.

21. Barrell, D., Litchfield, N., Townsend, D., Quigley, M., Van Dissen, R., Cosgrove, R., Cox, S., Furlong, K., Villamor, P., and Begg, J. (2011) Strike-slip ground-surface rupture (Greendale Fault) associated with the 4 September 2010 Darfield earthquake, Canterbury, New Zealand. *Quarterly Journal of Engineering Geology and Hydrogeology*, **44**, 283-291.

22. Blanchard, F. and Laverty, G. (1966) Displacements in the Claremont water tunnel at the intersection with the Hayward fault. *Bulletin of the Seismological Society of America*, **56**, 291-294.

23. Brown, I. and Brekke, T. (1980) Some aspects of the behaviour of tunnels that cross active faults. T*hird Australia-New Zealand Conference on Geomechanics*, Institution of Professional Engineers New Zealand, Wellington, N.Z., 189-194.

24. Caulfield, R.J., Kieffer, D.S., Tsztoo, D.F., and Cain, B. (2005) Seismic design measures for the retrofit of the claremont tunnel. *RETC Proceedings California*.

25. Lange, S., Mason, H.B., Scott, M.H., and Ashford, S.A. (2018) Analysis of concrete-lined tunnels crossing active faults. *North American Tunneling 2018 Proceedings*.

26. Shen, Y., Gao, B., Yang, X., and Tao, S. (2014) Seismic damage mechanism and dynamic deformation characteristic analysis of mountain tunnel after Wenchuan earthquake. *Engineering Geology*, **180**, 85-98.

27. Wang, Z., Gao, B., Jiang, Y., and Yuan, S. (2009) Investigation and assessment on mountain tunnels and geotechnical damage after the Wenchuan earthquake. *Science in China Series E: Technological Sciences*, **52**, 546-558.

28. Yashiro, K., Kojima, Y., and Shimizu, M. (2007) *Historical Earthquake Damage to Tunnels in Japan and Case Studies of Railway Tunnels in the 2004 Niigataken-Chuetsu Earthquake*. Quarterly Report of RTRI, **48**, 136-141.

29. Brown, I., Brekke, T., and Korbin, G. (1981) *Behaviour of the Bay Area Rapid Transit Tunnels through the Hayward Fault*. Final Report to the US Department of Transportation. Report No. UMTA-CA-06-0120-81-1.

30. ASCE (1984) *Guidelines for the Seismic Design of Oil and Gas Pipeline Systems*. American Society of Civil Engineers, Committee on Gas Liquid Fuel Lifelines.

31. ALA (2005) *Seismic Guidelines for Water Pipelines*. American Lifelines Alliance.

32. Hung, J., Monsees, J., Munfah, N., and Wisniewski, J. (2009) Technical manual for design and construction of road tunnels-civil elements. *Prepared for the US Department of Transportation*. Publication No. FHWA-NHI-10-034.

33. Power, M., Fishman, K.L., Makdisi, F., Musser, S., Richards Jr, R., and Youd, T.L. (2006) *Seismic Retrofitting Manual for Highway Structures: Part 2-Retaining Structures, Slopes, Tunnels, Culverts and Roadway*s. Technical Report MCEER-06-SP11, MCEER, University at Buffalo, The State University of New York.

34. Baziar, M.H., Nabizadeh, A., Khalafian, N., Lee, C.J., and Hung, W.Y. (219) Evaluation of reverse faulting effects on the mechanical response of tunnel lining using centrifuge tests and numerical analysis. *Géotechnique*, 1-13.

35. Mamaghanian, N., Jafari, M.K., and Kamalian, M. (2012) Effects of the tunnel presence on the pattern of the reverse faulting development on the ground surface. *The First National Conference on Urban Construction in the Vicinity of Active Faults*.

36. Ma, Y., Sheng, Q., Zhang, G., and Cui, Z. (2019) A 3D discrete-continuum coupling approach for

investigating the deformation and failure mechanism of tunnels across an active fault: a case study of xianglushan tunnel. *Applied Sciences*, **9**, 2318.

37. Shahidi, A. and Vafaeian, M. (2005) Analysis of longitudinal profile of the tunnels in the active faulted zone and designing the flexible lining (for Koohrang-III tunnel). *Tunnelling and Underground Space Technology*, **20**, 213-221.

38. Wang, Z., Zhang, Z., and Gao, B. (2012) Seismic behaviour of the tunnel across active fault. *The 15th World Conference on Earthquake Engineering*, Lisbon, Portugal, 24-28.

39. Karamitros, D., Bouckovalas, G., Kouretzis, G., and Gkesouli, V. (2011)An analytical method for strength verification of buried steel pipelines at normal fault crossings. *Soil Dynamics and Earthquake Engineering*, 31, 1452-1464.

40. Kennedy, R.P., Chow, A., and Williamson, R.A. (1977) Fault movement effects on buried oil pipeline. *Transportation Engineering Journal of the American Society of Civil Engineers*, **103**, 617-633.

41. Newmark, N.M. and Hall, W.J. (1975) Pipeline design to resist large fault displacement. *Proceedings of US national Conference on Earthquake Engineering*, 416-425.

42. Tohidifar, H., Moosavi, M., and Jafari, M.K. (2019) Nonlinear analysis of the surface faulting effects on the buried pipelines using the finite difference and multi-variable Newton methods. *Bulletin of Earthquake Science and Engineering*, Accepted for Publication.

43. Fib (2013) *Fib Model Code for Concrete Structures 2010, International Federation for Structural Concrete (fib)*. Wilhelm Ernst & Sohn, Germany.

44. McCormac, J.C. and Brown, R.H. (2013) *Design of Reinforced Concrete*. 9th Ed., Wile.

45. TEC (2016) *Tunnel Engineering Committee, Standard Specifications for Tunneling - 2016: Cut-and-Cover Tunnels*. Japan Society of Civil Engineers, Tokyo, Japan.

46. Eurocode2 (2004) *Design of Concrete Structures: Part 1-1: General Rules and Rules for Buildings*. British Standards Institution and European Committee for Standardization.

47. ITA (2000) *International tunnelling association, working group No. 2: guidelines for the design of shield tunnel lining. Tunnelling and Underground Space Technology*, **15**, 303-331.

48. ITA (1988) International tunnelling association, working group on general approaches to the design of tunnels: guidelines for the design of tunnels. *Tunnelling and Underground Space Technology*, **3**, 237-249.

49. ACI318 (2014) *Building Code Requirements for Structural Concrete (ACI 318-14): Commentary on Building Code Requirements for Structural Concrete (ACI 318R-14)*. ACI Report, American Concrete Institute. ACI.

50. Gere, J. and Timoshenko, S. (1997) *Mechanics of Materials*. PWS-KENT Publishing Company.

51. Wells, D.L. and Coppersmith, K.J. (1994) New empirical relationships among magnitude, rupture length, rupture width, rupture area, and surface displacement. *Bulletin of the Seismological Society of America*, **84**, 974-1002.